PCCP



PAPER

View Article Online

View Journal | View Issue



Cite this: Phys. Chem. Chem. Phys., 2018, 20, 10721

Kinetics of the $a-C_3H_5 + O_2$ reaction, investigated by photoionization using synchrotron radiation†

D. Schleier,^a P. Constantinidis,^a N. Faßheber,*^b I. Fischer, ^b * G. Friedrichs, ^b P. Hemberger, ^{*} * E. Reusch,^a B. Sztáray ^d and K. Voronova *

The kinetics of the combustion-relevant reaction of the allyl radical, a-C₃H₅, with molecular oxygen has been studied in a flow tube reactor at the vacuum ultraviolet (VUV) beamline of the Swiss Light Source storage ring, using the CRF-PEPICO (Combustion Reactions Followed by Photoelectron Photoion Coincidence Spectroscopy) setup. The ability to measure threshold photoelectron spectra enables a background-free detection of reactive species as well as an isomer-specific analysis of reaction products. Allyl was generated by direct photodissociation of allyl iodide at 266 nm and 213 nm and indirectly by the reaction of propene with Cl atoms, which were generated by photolysis from oxalyl chloride at 266 nm. Experiments were conducted at room temperature at low pressures between 0.8 and 3 mbar using Ar as the buffer gas and with excess O_2 to maintain nearly pseudo-first-order reaction conditions. Whereas allyl was detected by photoionisation using synchrotron radiation, the main reaction product allyl peroxy was not observed due to dissociative ionisation of this weakly bound species. From the concentration-time profiles of the allyl signal, second-order rate constants between $1.35 \times 10^{11}~\text{cm}^3~\text{mol}^{-1}~\text{s}^{-1}$ at 0.8~mbar and $1.75 \times 10^{11}~\text{cm}^3~\text{mol}^{-1}~\text{s}^{-1}$ at 3 mbar were determined. The rates obtained for the different allyl radical generation schemes agree well with each other, but are about a factor of 2 higher than the ones reported previously using He as a buffer gas. The discrepancy is partly attributed to the higher collision efficiency of Ar causing a varying fall-off behavior. When allyl is produced by the reaction of propene with Cl atom, an unexpected product is observed at m/z = 68, which was identified as 1,3-butadienal in the threshold photoelectron spectrum. It is formed in a secondary reaction of allyl with the OCCl radical, which is generated in the 266 nm photolysis of oxalyl chloride.

Received 23rd November 2017, Accepted 11th January 2018

DOI: 10.1039/c7cp07893e

rsc.li/pccp

Introduction

In this paper, we investigate the reaction of the allyl radical 1 with molecular oxygen, using photoelectron photoion coincidence spectroscopy and vacuum ultraviolet (VUV) synchrotron radiation (SR). This reaction is relevant in combustion chemistry, because 1 and other resonance-stabilized radicals¹ exhibit a low reactivity towards molecular oxygen, due to their comparably high thermodynamic stability. These radicals are produced abundantly as combustion intermediates¹ and through the hydrocarbon photolysis in planetary atmospheres.² Their ability to react with themselves and each other, resulting in the formation of

The allyl radical has been extensively studied by several research groups in the past. In the laboratory, it is commonly generated by pyrolysis or photolysis of suitable precursors such as propene or allyl halides. Its structure and its unimolecular reactions were assessed by various spectroscopic methods. ^{12,13} The excited state lifetimes and couplings, ¹⁴ the ionization energy (IE), ¹⁵ unimolecular reaction rates and reaction energetics ^{16,17} were measured. However, to understand the detailed kinetics of combustion processes, it is important to investigate the bimolecular reactions of 1. Rate constants for its self-reaction (dimerization) were determined by several groups. ^{18–21}

aromatic rings, can compete with oxidation processes, which makes them key species in molecular weight growth, *i.e.* soot formation.^{3–5} Allyl, in particular, appears in propene and 1-hexene flames⁶ and has also been detected in interstellar media⁷ and exoplanetary atmospheres.^{2,8,9} Furthermore it is involved in tropospheric reactions,¹⁰ and even in biological systems.¹¹ Reliable spectroscopic and kinetic data of 1 and its chemical reactions therefore contribute to our overall understanding of the reactivity of this important radical, providing input for predictive combustion and atmospheric models.

 ^a Institute of Physical and Theoretical Chemistry, University of Würzburg,
 Am Hubland, D-97074 Würzburg, Germany. E-mail: ingo.fischer@uni-wuerzburg.de
 ^b Institute of Physical Chemistry, Christian-Albrechts-University of Kiel, Max-Eyth-Str. 1,

Institute of Physical Chemistry, Christian-Albrechts-University of Kiel, Max-Eyth-Str. 1
 D-24118 Kiel, Germany. E-mail: fassheber@phc.uni-kiel.de
 Laboratory for Femtochemistry and Synchrotron Radiation, Paul Scherrer Institut

⁽PSI), CH-5232 Villigen, Switzerland. E-mail: patrick.hemberger@psi.ch

^d Department of Chemistry, University of the Pacific, Stockton, CA 95211, USA.

^d Department of Chemistry, University of the Pacific, Stockton, CA 95211, USA E-mail: kvoronova@pacific.edu

 $[\]dagger\,$ Electronic supplementary information (ESI) available. See DOI: 10.1039/c7cp07893e

The measured values were recently validated by multiplexed photoionization mass spectrometry (PIMS) utilizing VUV-SR.²²

The reaction of 1 with molecular oxygen (1)

$$a-C_3H_5 + O_2 \rightleftharpoons C_3H_5O_2 \quad \Delta_r H^\circ = -75.6 \text{ kJ mol}^{-1}$$
 (1)

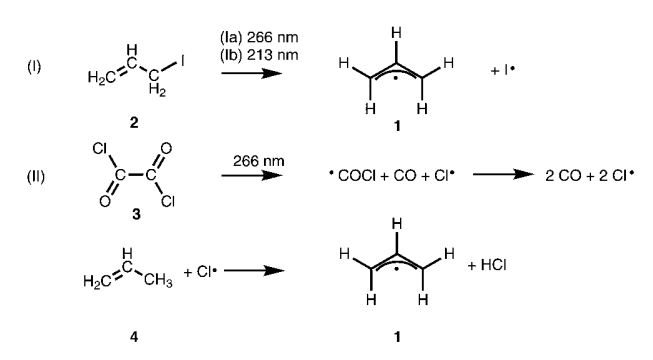
plays a critical role in combustion chemistry and has therefore been the focus of several computational and experimental studies.^{23–29} The first experiments determined the equilibrium constant between allyl and allyl peroxy at different temperatures and pressures and derived thermochemical parameters for reaction (1). 25,26 Interestingly, while alkyl compounds tend to react fast with oxygen at elevated temperatures, Morgan et al. showed that reaction (1) cannot be observed at temperatures above 573 K.24 The most comprehensive study on (1) was conducted by Rissanen et al.30 who studied the kinetics of the reaction from 201 K to 298 K in a flow reactor and measured the equilibrium constant for (1) between 320 K and 420 K. They photolysed allyl bromide at 193 nm, detected the allyl radical by photoionisation using a discharge lamp and monitored the allyl signal decay via time-resolved mass spectrometry. Notably, they did not observe a signal from allyl peroxy, the assumed main reaction product, in their experiments.

Synchrotron light sources offer superior photon intensities and tunability for photoionisation detection, and are especially well suited for detection of transient species in low concentrations.^{31–34} Tunable VUV radiation offers further benefits for isomer-specific product detection, based on the photoionisation spectrum (also called photoionisation efficiency curve) and identification in multiplexed time- and photon-energy resolved PIMS (photoionisation mass spectrometry) experiments.35 The technique is currently the gold standard as a sensitive and selective tool to monitor all products of a gas-phase chemical reaction in parallel, leveraging the multiplex advantage of time-of-flight mass spectrometry.³⁶ This technique has been pioneered for the study of chemical kinetics, initiated by photolysis in a "slow-flow" chemical reactor, by Osborn, Taatjes, and co-workers, 37 who also investigated the allyl self-reaction, vide supra.²² Recently, a new instrument^{38,39} was built at the VUV beamline⁴⁰ of the Swiss Light Source (SLS), which offers higher isomer selectivity by also recording the photoion mass-selected threshold photoelectron spectrum (ms-TPES).41 In the CRF-PEPICO (Combustion Reactions Followed by Photoelectron Photoion Coincidence) setup the radicals are generated in a laser photolysis flow reactor system coupled to a novel electron and ion optics setup that features dual velocity map imaging and cation space focusing. The properties of the new setup were recently demonstrated by measuring the ms-TPES of propargyl and iodomethyl radicals,³⁸ offering new insights into the vibrational structure observable only at room temperature (or colder) samples. In addition, the capabilities of the new experiment to measure concentrationtime profiles and hence to perform reaction kinetics studies were illustrated in the reaction of the CH₂I radical with oxygen, although only traces of the highly coveted CH2OO Criegee intermediate could be detected.³⁸ Moreover, the simplest alkylperoxy radical, CH₃OO, was also studied using the new CRF-PEPICO apparatus. 42 It was shown that statistical simulations of the breakdown diagram can serve as molecular thermometer of free radicals, which can be used to monitor the thermal equilibrium of these species – a continuous issue in kinetic experiments.

In the experiment described here, we have reinvestigated the reaction between molecular oxygen and the allyl radical to (a) characterise the setup for future investigations, (b) to complement the existing data at low pressures (c) to systematically investigate and compare the various methods to generate allyl radicals for kinetics experiments, and (d) to further explore why the allyl peroxy product has not been observed in previous experiments. In the experiments described below we use three different photolysis schemes to generate allyl: photolysis of halide precursors at (Ia) 266 nm and (Ib) 213 nm as well as the propene + Cl reaction (II), using Cl atoms formed at 266 nm.

Experimental

Experiments were performed using the new double imaging CRF-PEPICO spectrometer³⁸ at the VUV beamline⁴⁰ of the Swiss Light Source (SLS). The instrument has been described in detail elsewhere, 38 thus only a brief overview is given here. The CRF-PEPICO utilizes a side-sampled flow tube chemical reactor coupled with electron and ion optics that simultaneously achieve velocity map imaging and Wiley-McLaren⁴³ space focusing of photoions. The approaches to generate 1 are illustrated in Scheme 1 and include direct photolysis of allyl iodide 2 at 266 nm (Ia) as well as at 213 nm (Ib) and formation of 1 from the reaction of propene 4 with chlorine atoms (II), which are generated by photolysis from oxalyl chloride 3 at 266 nm. The 4th (around 150 mJ cm⁻²) and 5th (around 30 mJ cm⁻²) harmonic of a 20 Hz Nd:YAG laser were used for photolysis. Calibrated mass flow controllers were employed for all reactants. The vapour of 2 was introduced into the flow tube by a metered flow of 1 bar Ar through a glass container filled with liquid 2, assuming a vapour pressure of 51 mbar. To adjust mole fractions, it was mixed in situ with a metered flow of argon and introduced into the 57.4 cm long, 1.25 cm (1/2'') I.D. quartz tube reactor, coated with halocarbon wax and mounted parallel to the synchrotron beam. The pressure in the reactor tube p_R was kept between $p_{\rm R}$ = 0.8–3 mbar by throttling to vacuum at the flow tube exit.



Scheme 1 The allyl radical 1 was generated either by direct photolysis of allyl iodide 2 (I) or by the reaction of propene 4 with Cl atoms (II).

In Scheme 1 (II) 9% of $\bf 3$ and 1% of $\bf 4$ were introduced to the mixture.

The total gas flow rate was set high enough to completely replace the gas mixture in the reactor tube with a fresh sample in-between two consecutive laser pulses in order to avoid accumulation of reaction products. The laser beam propagated down the reactor and is assumed to create a uniform density of photolysis products, which were then sampled into the ionization region through a 300 μm pinhole at the halfway point of the tube. The pressure in the ionization chamber was kept below 7×10^{-6} mbar, which limited $p_{\rm R}$ to a few mbar.

Concentrations of all precursor compounds were determined from their partial pressures, using the ideal gas law. Concentrations of 1 and I atoms were determined using the depletion of the precursor signal upon photolysis. The photon energy was calibrated on the Ar 11s'-14s' autoionization lines in the first and second order of the monochromator grating. Higher harmonic radiation was suppressed by a MgF2 window or a rare gas filter. The effusive gas beam was crossed by the VUV radiation at a distance of 21 \pm 4 mm from the flow tube and a constant extraction field of 125 V cm⁻¹ (experiments (Ia) and (II)) or 250 V cm⁻¹ (experiment (Ib)) accelerated the generated photoions and photoelectrons in opposite directions towards the Roentdek DLD40 position-sensitive delay-line detectors. In this setup, the electron-hit times provide a start signal for the ion time-of-flight mass analysis in a multiple-start/multiple-stop data acquisition scheme.44 The VUV photon energy was scanned between 8.0-8.5 eV to record a TPES of the allyl radical using experimental conditions (Ib) and (II). Threshold electrons were selected with an energy resolution of 5 meV and the contribution of hot electrons was subtracted, following the procedure given in ref. 45. Each full scan consists of a multi-dimensional data set, which yields time-of-flight mass spectra, threshold photoelectron spectra, and reaction kinetic traces.

To obtain kinetic traces, the coincidence intensity of the allyl time-of-flight signal was plotted as function of the reaction time (difference between the coincidence and laser time stamps). The data were averaged for 13-90 minutes at a photon energy of 9.0 eV. The detailed experimental conditions are given in Table S1 in the ESI.† The concentrations of 2 or 4 were chosen so that the allyl radical decay time did not depend on the precursor concentration. At the beginning and at the end of each set of experiments, the radical loss rates were recorded with no oxygen present to quantify side reactions and wall loss processes. The allyl radical concentration was calculated from the coincidence spectra, based on the depletion of the precursor signal with photolysis laser on and off. In the next step, the rate constant k_1 was measured as a function of O_2 concentration, which was at least one order of magnitude higher than the allyl radical concentration, to maintain pseudo-first-order conditions. Kinetic traces were analysed using the CHEMKIN-II package⁴⁶ and SENKIN routine.⁴⁷ For sensitivity analysis, the sensitivity coefficient $\sigma(i,j,t)$ for reaction i of species j at time t was normalized with respect to the maximum concentration c_{max} of the species j over the time history, $\sigma(i,j,t) = 1/c_{\text{max}} \times (\partial c(j,t)/\partial \ln k_i)$. The kinetic time resolution of the experiment was limited by the spread in the time it takes for the test gas to travel from the pinhole of the reactor to the ionisation point. It was accounted for by convoluting the concentration–time profiles with a Maxwell–Boltzmann type response function with 1 ms FWHM (full width at half maximum), see Fig. S1 in the ESL† Rate constants were optimised by iteratively fitting the convoluted concentration–time profiles to the experimentally observed kinetic profiles using a Levenberg–Marquardt least-squares fitting algorithm. The respective rate constant value and the conversion factor that was applied to convert the total MS counts into allyl concentration were used as the fitting parameters.

Results and discussion

1. Photolysis of allyl iodide

In a first series of experiments, **1** was generated by photolysis of **2** at either 266 nm or 213 nm, see (Ia) and (Ib) in Scheme **1**. The allyl iodide/Ar mixture contained 0.5% of **2**. From the depletion of the precursor signal with the photolysis laser turned on, we derived a conversion efficiency of 0.5% at 266 nm and 5% at 213 nm. Note that for **2** absorption cross sections of 1.6 Mb⁴⁸ or **2**.3 Mb²⁹ at 266 nm and 16 Mb at 213 nm²⁹ were reported.

Mass spectra. The coincidence time-of-flight (mass) spectrum recorded at 9.0 eV upon photolysis of 2 (Fig. 1) exhibits two distinct peaks, one at m/z = 168, corresponding to 2 and the other one at m/z = 41, due to 1. Note that the IE of 2 is 9.30 eV,⁴⁹ so precursor molecules can only be ionised by residual higher harmonic radiation or if they are vibrationally highly excited. Therefore, the ion signal of 2 is small. At higher photon energies (>10.5 eV), ionised iodine atoms were detected as well. Recombination products such as 1,5-hexadiene and I2 were observed at photon energies above 9.5 eV, but their signals were too small to record a TPES or evaluate the kinetics. Note that the appearance energy (AE) for the formation of the allyl cation 1⁺ through the ionic dissociation of allyl iodide 2⁺ is 9.80 eV, 50 hence the background-free analysis of the allyl signal is limited to lower photon energies. To characterise the source of the m/z = 41 signal, a ms-TPES was recorded (cf. Fig. S2 in the ESI†), which agrees well with the earlier one of allyl⁵¹ and thus indicates that the m/z = 41peak is indeed coming from 1, vide infra.

In agreement with previous experiments, no $\rm C_3H_5O_2$ or $\rm C_3H_5O$ signal was observed in the mass spectra upon oxygen addition.

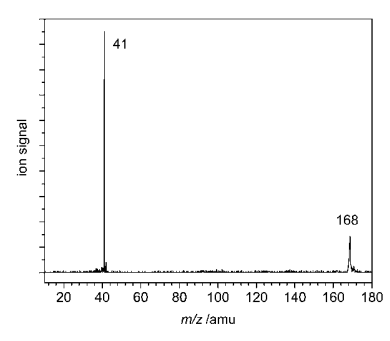


Fig. 1 Sample time-of-flight mass spectrum measured after allyl iodide photolysis (266 nm) at 9.0 eV.

Calculations by Lee and Bozelli²³ on the allyl peroxy radical revealed a shallow potential well of C₃H₅O₂ but high barriers to secondary reaction products. We carried out CBS-QB3 calculations on the lowest-energy rotamer, which revealed a triplet ground state for allyl peroxy cation and an adiabatic ionisation energy of IE = 8.89 eV. Due to a strong increase of the C-O bond length upon ionisation, the Franck-Condon factors are small for transitions into the lowest triplet ion state. In addition, the binding energy of the cation is calculated to be only 60 meV and an appearance energy $AE_{0K}(C_3H_5O_2, C_3H_5^+)$ of 8.95 eV (CBS-QB3) is expected from the computations, rendering it difficult to detect the intact ion. According to the literature two effects can explain this finding: Firstly, ionization takes place from the HOMO-1 (highest molecular orbital-1), which is a bonding orbital with respect to the C-O bond. Secondly, the allyl cation is resonantly stabilised after C-O bond cleavage. Therefore the binding energy is small and the allyl peroxy radical cannot be observed easily by photoionisation. 52 Two more isomers of $C_3H_5O_2$ exist, which are presumably more stable, but cannot be formed from allyl.

Reactions without O_2 . Several reactions, including recombination reactions, may contribute to the decay of photolytically formed allyl radical and have to be taken into account in the analysis of reaction (1). To quantify these side reactions, the decay kinetics of the allyl signal was measured without the presence of O_2 . A typical decay profile of the allyl radical is given in the upper trace of Fig. 2 (red dots). Note that, despite instantaneous allyl radical formation by photolysis, the apparent slow initial increase of the allyl signal is due to the kinetic time resolution of the experimental setup. To fit the experimental data, the most likely side reactions were taken into account with fixed rate constants as a background mechanism, and the remaining discrepancies between modelled and measured allyl radical loss were attributed to a first-order wall loss process. An overview of the key reactions is given in Table 1.

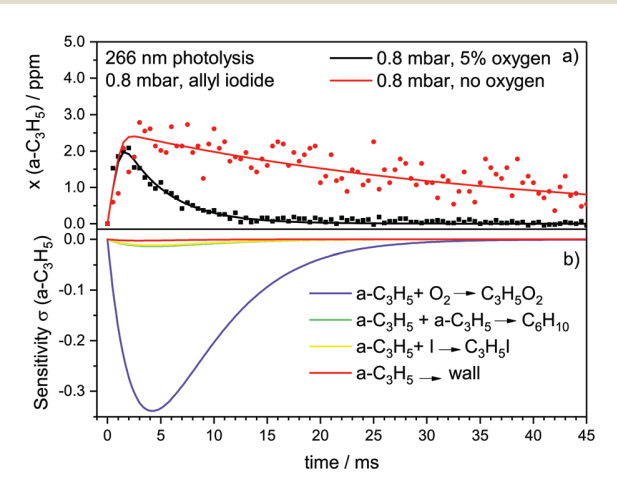


Fig. 2 (a) Example for a decay curve of the allyl radical signal. Symbols refer to experimental data, solid lines represent fits from numerical simulations accounting for the convoluted response function. The sensitivity analysis depicted in trace (b) illustrates the influence of the four most important reactions on the experiment with 5% oxygen in the reaction mixture and indicate the minor importance of secondary chemistry.

Table 1 Background reactions included in the analysis of the decay of the allyl signal, using photolysis of 2

No.	Reaction	Rate constant k	Ref.
(2) (3)	$\begin{array}{c} \text{2a-C}_{3}\text{H}_{5} \to \text{C}_{6}\text{H}_{10} \\ \text{a-C}_{3}\text{H}_{5} + \text{I} \to \text{C}_{3}\text{H}_{5}\text{I} \end{array}$	$1.63 \times 10^{13} \text{ cm}^3 \text{ mol}^{-1} \text{ s}^{-1}$ $1.0 \times 10^{14} \text{ cm}^3 \text{ mol}^{-1} \text{ s}^{-1}$	Selby <i>et al.</i> ²² Jenkin <i>et al.</i> ²⁹
. ,	$a-C_3H_5 \rightarrow wall$	9 s ⁻¹ (213 nm) 20 s ⁻¹ (266 nm)	This work
(5)	$I + I + M \rightarrow I_2 + M$	$2.96 \times 10^{15} \text{ cm}^6 \text{ mol}^{-2} \text{ s}^{-1}$	Baulch et al.53

The rate constant for the dimerization of two allyl radicals, yielding hexadiene (2) was taken from the work by Selby et al. (vide supra) conducted at pressures between 1-6 Torr at 298 K.²² As their value was obtained at conditions similar to our experiments, it was used without any correction. For the back reaction (3) between 1 and I atoms, Jenkin et al. reported a value of 9.6 \times 10¹³ cm³ mol⁻¹ s⁻¹.²⁹ Selby *et al.* noted that during their experiments with allyl bromide and chloride similar values were obtained.²² We fixed the rate at a value of $1.0 \times 10^{14} \text{ cm}^3 \text{ mol}^{-1} \text{ s}^{-1}$, in agreement with ref. 29. As the decay of 1 was already well described by reactions (2) and (3), the rate for wall loss obtained from the fit was small and had no significant impact on the overall kinetics. The dimerization of I to I_2 (5) was also included in the kinetic model, because it has a feedback on the recombination reaction (3). The best fit is given by the solid red line in the upper trace of Fig. 2.

Reactions with O_2. In the next series of experiments, 1, 2, 5, 7.5 and 10% of O2 was added, while maintaining a total flow tube pressure of $p_R = 0.8$ mbar. In the presence of molecular oxygen, reaction (1) now constitutes a new pathway for the decay of 1. As an example, the data points for $x(O_2) = 5\%$ are given as black squares in the upper trace of Fig. 2. The allyl signal decays to the background level, indicating that it is completely consumed under the reaction conditions and that fragment ion signals of potential secondary products do not interfere with the allyl radical detection. The background mechanism utilized to fit the data of the allyl signal decay in the absence of oxygen was used to model reaction (1). For the reverse of (1), we estimated a rate between 0.25 (at 0.8 mbar) and $0.48~{
m s}^{-1}$ (at 3 mbar) from the thermodynamic data in the literature, 30 which is negligible under the reaction conditions applied and agrees with previous reports. 23,24,29 Fig. 2(b) depicts a sensitivity analysis, which illustrates the influence of reactions (1)-(4) on the simulation of the allyl radical decay. The high values of the sensitivity coefficient of reaction (1) show that the simulated decay almost entirely depends on the chosen value for the rate constant of the reaction (1). Therefore, possible deviations of the rate constants for the side reactions (2) to (4) from the values given in Table 1 have only a minor impact on the determined rate constant. Fig. S4 (ESI†) shows a similar analysis for data obtained upon 213 nm photolysis.

Pseudo-first-order conditions were maintained with $[O_2]$ being always at least an order of magnitude larger than [allyl]. In a pseudo-first-order plot manner, Fig. 3 displays corresponding first-order rate constants $k^{1\text{st}}$, which have been simply derived from the fitted values by $k^{1\text{st}} = k_1 \times [O_2]$. In case of consistent k_1 values, the data points should yield a linear plot

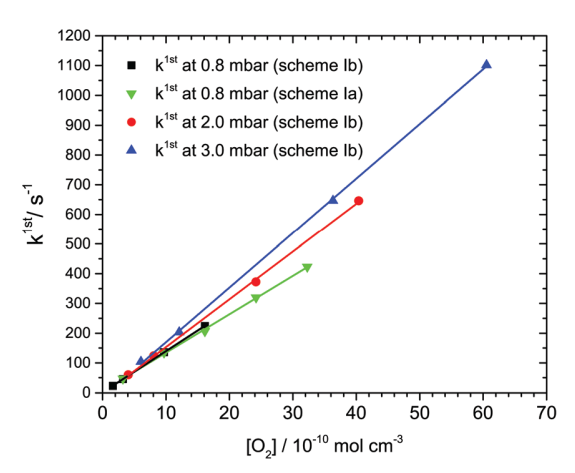


Fig. 3 Pseudo-first-order plot of rate constants determined for buffer gas pressures of 0.8, 2.0, and 3.0 mbar using precursors **2** and **4** at two different photolysis wavelengths.

with zero y-axis offset and the average k_1 as the slope, which is actually the case within error limits. The least square fit of the data obtained at $p_{\rm R}=0.8$ mbar and 266 nm (green triangles) yield $k_1=(1.29\pm0.02)\times10^{11}~{\rm cm}^3~{\rm mol}^{-1}~{\rm s}^{-1}$, where the error indicates the statistical 2σ standard error of the slope. Note that a simple averaging of the original k_1 data would have yielded $k_1=(1.35\pm0.07)\times10^{11}~{\rm cm}^3~{\rm mol}^{-1}~{\rm s}^{-1}$, in quantitative agreement within error limits. The first- and second-order rate constants derived in the individual experiments are summarised in Tables S2 and S3 in the ESI.†

2. Propene & oxalyl chloride

Generation of 1 from propene 4 via reaction (II) provides an alternative pathway for allyl radical formation. Oxalyl chloride ((COCl)₂) 3 is commonly used as a photolytic precursor of Cl atoms in kinetic and photochemical studies. ^{49,54,55}

Suits and co-workers studied the 235 nm⁵⁶ and 193 nm⁵⁷ photolysis of 3 and found that the dissociation initially yields Cl, CO and OCCl in a first fast reaction step, followed by a slow dissociation of most of the remaining OCCl to Cl and CO. However, Wu *et al.* did not observe IR emission of OCCl produced by 193 nm⁵⁸ and 248 nm⁵⁹ photolysis, indicating that the initially formed OCCl decomposes rapidly to Cl and CO on the timescale of a typical kinetic experiment. Baklanov and Krasnoperov⁶⁰ reported a total quantum yield of 2 for Cl atoms from 193 nm (COCl)₂ dissociation and determined absorption

cross-sections of 3 between 193 and 390 nm. Gosh $et~al.^{61}$ investigated the Cl quantum yields using pulsed laser photolysis combined with atomic resonance fluorescence (PLP-RF) for 193, 248 and 352 nm photodissociation of 3. Moreover, they measured the rate constants for the thermal decomposition of OCCl at temperatures of 253 K and 298 K at total pressures between 17 and 170 mbar. They also found a total (i.e., including Cl from consecutive thermal decomposition) quantum yield for Cl of about 2 at all three wavelengths. Very recently, Huang et~al. questioned this result based on their exploration of a direct Cl₂ elimination pathway at 248 nm photolysis. They detected Cl₂ by cavity ringdown spectroscopy and reported a small but significant Cl₂ formation with a quantum yield of >0.14.

In this work, we relied on the absorption cross section of 0.15 Mb reported for 270 nm photolysis by Gosh $et\ al.^{61}$ We estimated the Cl atom photolysis yield for 266 nm using the 270 nm absorption cross-section, which is 15 times lower than that of allyl iodide. Hence, it was assumed that 0.03% of the (COCl)₂ decomposed to Cl, CO and OCCl with a quantum yield of 1, and the subsequent Cl formation by thermal decomposition of OCCl, reaction (6) was taken into account in the reaction mechanism (see Table 2) with the rate constant taken from Gosh $et\ al.^{61}$

A sample time-of-flight mass spectrum recorded at 9 eV photon energy of the Cl atom initiated allyl radical formation from propene is shown in Fig. 4. The spectrum is dominated by the allyl cation $\mathbf{1}^+$ signal at m/z = 41, and the photolysis product of oxalyl chloride, m/z = 63 and 65, OC³⁵Cl and OC³⁷Cl, respectively.

The presence of $(COCl)_2$ 3⁺ $(m/z = 126 (C_2O_2^{35}Cl_2), 128$ $(C_2O_2^{35}Cl^{37}Cl)$, 130 $(C_2O_2^{37}Cl_2)$) and propene 4⁺ (m/z = 42)cations is not expected at this photon energy, since their ionisation energy are 10.91 eV⁶³ and 9.74 eV,⁶⁴ respectively. However, it can be explained by the small amounts of highenergy photons present in the monochromatised synchrotron beam (white light scattered by the grating), and by 3 and 4 being the most abundant species in the reactor. In addition, the dissociative photoionisation products of oxalyl chloride, m/z =91 ($C_2O_2^{35}Cl$), 93 ($C_2O_2^{37}Cl$), 98 ($CO^{35}Cl_2$), 100 ($CO^{35}Cl^{37}Cl$), 102 (CO³⁷Cl₂), are also visible in the mass spectrum due to the residual high-energy photon radiation. Note that several possible reaction products such as Cl, Cl₂, HCl and CO have ionisation energies above 9 eV. However, a series of small peaks extending from m/z = 35 to 38 are probably due to Cl and HCl, again ionised by higher harmonics.

Table 2 Reaction mechanism for determination of reaction (1) from the 266 nm photolysis of oxalyl chloride/propene mixtures in Ar

No.	Reaction	k	Ref.
(2) (4) (6) (7) (9a) (9b)	$\begin{array}{c} 2\text{a-}C_{3}H_{5} \to C_{6}H_{10} \\ \text{a-}C_{3}H_{5} \to \text{wall loss} \\ \text{OCCl} \to \text{CO} + \text{Cl} \\ \text{Cl} + \text{Cl} + \text{M} \to \text{Cl}_{2} + \text{M} \\ \text{C}_{3}H_{6} + \text{Cl} \to \text{C}_{3}H_{6}\text{Cl} \\ \text{C}_{2}H_{6} + \text{Cl} \to \text{a-}C_{3}H_{5} + \text{HCl} \end{array}$	1.63 × 10 ¹³ cm ³ mol ⁻¹ s ⁻¹ 20 s ⁻¹ (at 0.8 mbar) 1600 s ⁻¹ 4.6 × 10 ¹⁵ cm ⁶ mol ⁻² s ⁻¹ 5.12 × 10 ¹² cm ³ mol ⁻¹ s ⁻¹ 2.23 × 10 ¹³ cm ³ mol ⁻¹ s ⁻¹	Selby <i>et al.</i> ²² This work Ghosh <i>et al.</i> , ³ extrapolated to 1 mbar Baulch <i>et al.</i> ⁵³ Kaiser and Wallington ⁶⁷ Kaiser and Wallington ⁶⁷
(10) (11)	$a-C_3H_5 + M \rightarrow \text{products} + M$ $O_2 + Cl + M \rightarrow ClO_2 + M$	$1.3 \times 10^9 \text{ cm}^3 \text{ mol}^{-1} \text{ s}^{-1}$ $5.8 \times 10^{14} \text{ cm}^6 \text{ mol}^{-2} \text{ s}^{-1}$	This work Atkinson <i>et al.</i> ⁶⁸

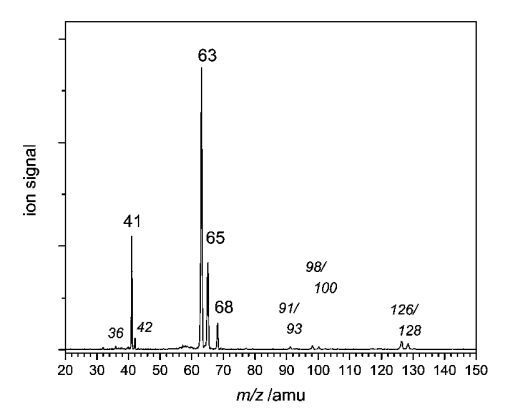


Fig. 4 Time-of-flight mass spectrum of a propene and (COCI)₂ mixture irradiated with 266 nm, recorded at 9.0 eV and $\rho_R = 1.0$ mbar.

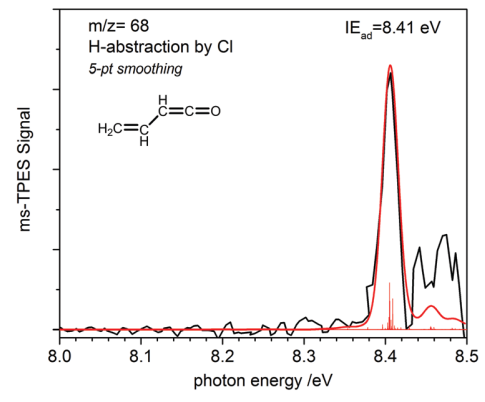


Fig. 5 The ms-TPES of the m/z = 68 signal is assigned to 1,3-butadienal. The red line represents a Franck-Condon simulation.

An additional peak with significant intensity appears at m/z=68, corresponding to $\rm C_4H_4O$ cations. To identify this species, a ms-TPES (Fig. 5) was recorded, which shows a peak at 8.41 eV corresponding to the IE. Ionisation energies are available for a number of isomers. The only one with an IE close to the present value is 1,3-butadienal, also termed vinylketene, with an IE of 8.4 eV reported from a conventional photoelectron spectrum. ⁶⁵ CBS-QB3 computations yielded an IE $_{\rm ad}=8.41$ eV in excellent agreement with the spectrum. The red line in Fig. 5 represents a Franck–Condon simulation, which matches the low-energy part of the spectrum well. We therefore assign the peak at m/z=68 to this isomer. Pathways for its formation are discussed below.

Reactions without O_2 . While the hydrogen abstraction by the Cl atom will preferentially take place at the methyl group of propene, H-abstraction at other positions leading to 1- or 2-propenyl is also possible. However, the PEPICO setup allows us to identify the radical unambiguously. In Fig. 6, a ms-TPES of m/z=41 is presented, which agrees very well with the earlier spectrum of the allyl radical, given in the lower trace of Fig. 6. ⁵¹ The first peak at 8.13 eV corresponds to the ionisation energy of 8.1309 eV. ¹⁵ Further peaks appear with a spacing of 55 meV and are due to a vibrational progression in the CCC bending mode ν_7^+ .

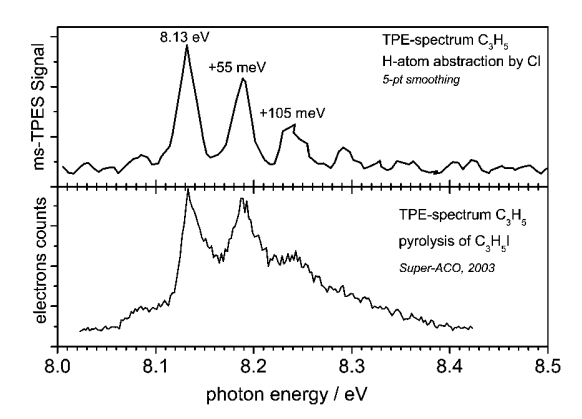


Fig. 6 Upper trace: The ms-TPES of the m/z=41 signal generated by the Cl atom initiated radical formation from propene. Lower trace: TPES of allyl from ref. 51.

Actually, the peaks are better resolved than in previous experiments using pyrolysis,⁵¹ which indicates better cooling of the radical in the present photolysis experiment. The spectrum in Fig. 6 proves that the allyl radical is the only carrier of the m/z = 41 peak in this photon energy range.

Due to the more complex allyl radical formation by Cl atom initiated H-abstraction (approach (II), Scheme 1) and due to the oxalyl chloride 3 photolysis leading to a simultaneous C–Cl and C–C bond cleavage generating Cl, CO, and OCCl radicals as outlined above, the formation of several side products had to be taken into account in the reaction mechanism (Table 2). The generated allyl radicals can be consumed in reactions with Cl and OCCl forming allyl chloride, C₃H₅Cl, by the dimerization of two allyl radicals to hexadiene, (2), and by the reaction with HCl. Chlorine atoms can recombine to Cl₂,

$$Cl + Cl + M \rightarrow Cl_2 + M$$
 (7)

or react with unconverted oxalyl chloride according to

$$Cl + (COCl)_2 \rightarrow Cl_2 + (CO)_2Cl$$
 (8)

the latter decomposing to OCCl and CO. Furthermore, by Cl atom addition to the double bond of propene, C_3H_6Cl can be formed. The reaction of 4 with Cl atoms was investigated by Kaiser and Wallington⁷ using FTIR and GC analysis. They reported rate constant data (see Table 2) and pressure dependent branching ratios between 0.4 and 933 mbar for the two possible reaction channels

$$C_3H_6 + Cl \rightarrow C_3H_6Cl$$
 (9a)

$$C_3H_6 + Cl \rightarrow C_3H_5 + HCl$$
 (9b)

with channel (9b), which leads to allyl formation being about 4 times faster than channel (9a) at 1 mbar.

To account for all possible additional allyl loss reactions, next to allyl dimerisation and wall loss (4) as also assumed for the allyl iodide experiments, we introduced an additional lump loss reaction,

$$a-C_3H_5 + M \rightarrow products + M$$
 (10)

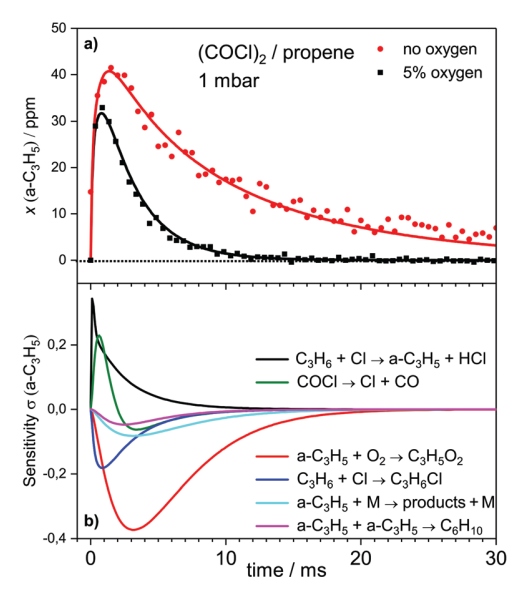


Fig. 7 (a) Experimental concentration—time profiles of the allyl radical generated by Cl atom initiated H-abstraction of propene, with no oxygen (red) and 5% oxygen (black) added. The solid lines denote numerical simulations. (b) Corresponding sensitivity analysis of the experiment with 5% oxygen.

and used its rate constant as a fit parameter to simulate the experimental allyl concentration–time profiles for the oxalyl chloride/propene mixtures without oxygen. A typical allyl concentration–time profile and its simulation are shown by red symbols and the red solid line in Fig. 7a, respectively. Other processes, such as the recombination of OCCl radicals to oxalyl chloride and the reaction between OCCl and Cl to phosgene 66 have been neglected. They do not have an influence on the overall allyl kinetics.

As already mentioned above, in the mass spectrum (Fig. 4) a peak at m/z = 68 is visible, which was identified as 1,3-butadienal based on its ms-TPES. A kinetic trace (Fig. S3, ESI†) shows that it is a product formed upon photolysis of (COCl)₂. There are several possible reactions that might form it in a mixture of 3 and 4, two of them starting from propene:

$$C_3H_6 + OCCl \rightarrow C_4H_4O + HCl + H$$
 (12)

$$C_3H_6 + COCl_2 \rightarrow C_4H_4O + 2HCl$$
 (13)

While (12) is thermochemically probably not favourable, because a radical is formed on the product side, (13) is not likely, because phosgene, $COCl_2$ will only be formed in minor amounts. Note that no heats of formation $\Delta_f H^\circ$ are available for 1,3-butadienal. Alternatively, it can be formed in a secondary radical–radical reaction of allyl, according to

$$a-C_3H_5 + OCCl \rightarrow C_4H_4O + HCl$$
 (14)

This reaction is expected to be highly exothermic and to proceed without a significant barrier. With an assumed and sufficiently long thermal lifetime of OCCl (about 0.6 ms, see Table 2), reaction (14) is also feasible in terms of OCCl abundance in the reaction mixture. We therefore assume that

1,3-butadienal is formed by reaction (14) and attachment of OCCl at one of the terminal carbon atoms.

Reactions with O_2 . Once a suitable kinetic model was established to model the allyl decay without oxygen present in the reaction mixture (red curve in Fig. 7a), oxygen was added and the resulting allyl profiles were fitted by adjusting the rate constant of reaction (1). Only the reaction

$$Cl + O_2 + M \rightarrow ClO_2 + M$$
 (11)

has been added to the mechanism to account for possible Cl loss due to the fairly high oxygen mole fractions. The black squares and black solid curve in Fig. 7a illustrate the concentration–time profile of 1 for an experiment with 5% oxygen as well as the corresponding sensitivity analysis in Fig. 7b. The sensitivity analysis reveals that a number of reactions is important for a correct description of the overall allyl yield, however, at reaction times > 2 ms the target reaction (1) becomes the most important allyl loss reaction. Overall, a bimolecular rate constant of 1.43×10^{11} cm³ mol⁻¹ s⁻¹ was obtained.

Alternatively, in order to test the importance of the assumed Cl concentration, the experiments were also analysed using a direct Cl quantum yield of 2 (instead of using a direct quantum yield of 1 with consecutive Cl formation from OCCl decomposition). This analysis lead to essentially the same result ($k_1 = 1.40 \times$ 10¹¹ cm³ mol⁻¹ s⁻¹). Finally, instead of estimating the photolysis efficiency of 0.03% as outlined above, as a third analysis strategy we simply adopted the conversion factor that was used before to convert the total MS counts into allyl concentration from the experiments with allyl iodide. In order to be able to simulate the resulting allyl concentration peak, about two times higher initial Cl atom concentrations had to be assumed. Nevertheless, again almost the same value (k_1 = 1.44 \times $10^{11}~\text{cm}^3~\text{mol}^{-1}~\text{s}^{-1})$ was determined for the rate constant of (1) indicating that the quantitative knowledge of the total Cl atom yield was not a crucial issue for the rate constant determination.

Comparison of data and pressure dependence. Rate constants of reaction (1), which have been measured at reactor pressures of $p_{\rm R}$ = 0.8, 1.0, 2.0, and 3.0 mbar, are shown in Fig. 8 as filled symbols and are summarised in Table 3. The obtained data using different allyl radical precursors show a very good agreement, hence demonstrating the reliability of the different kinetic evaluation schemes. Keeping in mind the more complex modelling of the allyl kinetic trace in case of the oxalyl chloride/propene system, photolysis of allyl iodide may serve as the preferred choice for kinetic experiments.

The data in Fig. 8 reveal a weak pressure dependence of the second-order rate constant, which is consistent with an association reaction in the fall-off regime. A simple association reaction according to

$$a-C_3H_5 + O_2 (+M) \rightarrow C_3H_5OO (+M)$$
 (1)

is in line with the results of the QRRK/ME (quantum Rice-Ramsperger-Kassel/master equation) study of the reaction system performed by Lee and Bozzelli.²³ Based on CBSQ//B3LYP/6-31G(d,p) composite calculations and at density functional

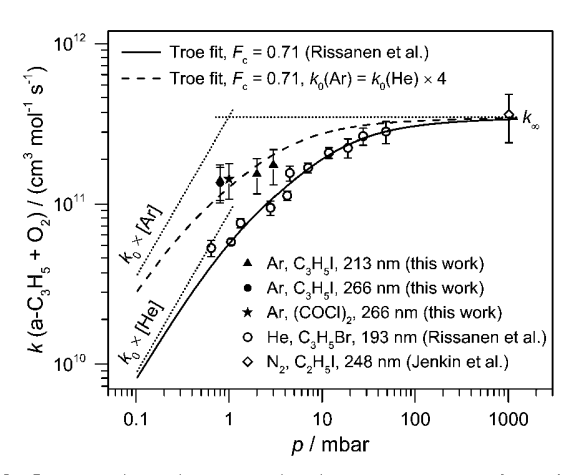


Fig. 8 Pressure dependent second-order rate constants of reaction (1) (filled symbols) determined using different allyl radical generation schemes in comparison with previous data reported by Rissanen $et~al.^{30}$ and Jenkin et~al. (open symbols)²⁹ Error bars correspond to the total estimated error in case of this study and Jenkin et~al. and the statistical 2σ standard error in case of Rissanen et~al. The solid and dashed lines represent a Troe fit of the fall-off behaviour (see text), the dotted lines are the respective high and low pressure limiting rate constants k_0 and k_∞ .

Table 3 Comparison of the second order rate constants for several pressures obtained for the different methods of allyl generation

Precursor	Pressure/mbar	Rate constant $k_1/\text{cm}^3 \text{ s}^{-1} \text{ mol}^{-1}$
2 (266 nm)	0.8	1.35×10^{11}
2 (213 nm)	0.8	1.40×10^{11}
,	2.0	1.54×10^{11}
	3.0	1.75×10^{11}
3, 4	1.0	1.43×10^{11}

levels of theory, they concluded that the association pathway dominates the room temperature reaction. Exit channels of possible H-shift isomerisation and cyclisation steps exhibit significant energy barriers of $>59~\rm kJ~mol^{-1}$ (with respect to the entrance energy) and are therefore not accessible at room temperature. With increasing temperature, however, due to the weakly bound $\rm C_3H_5OO$ with a dissociation barrier of only 84 kJ $\rm mol^{-1}$, the reverse reaction becomes important and equilibration of a-C₃H₅ + O₂ and C₃H₅OO can be observed as reported in the work of Rissanen *et al.*³⁰

The pressure-dependent room temperature rate constant data of Rissanen et~al. (open circles in Fig. 8)³⁰ are about a factor of two lower but show a comparable pressure dependence. Another single data point taken from Jenkin et~al.,²⁹ measured at atmospheric pressure (open diamond) has been included in Fig. 8 as well. The solid line represents the Troe fit⁶⁹ of the fall-off curve reported by Rissanen et~al.,³⁰ yielding a high pressure limiting rate constant k_{∞} that is in line with the atmospheric pressure value of Jenkin et~al.²⁹ While the value of k_{∞} is independent of the used buffer gas, the fall-off critically depends on the collision efficiency β_c of the bath gas molecules. It is defined as $\beta_c = k_0/k_0^{\rm sc}$ and $k_0^{\rm sc}$ corresponds to the low pressure rate constant in the strong collision limit, i.e. assuming that each collision causes stabilization of the initially formed

 $C_3H_5OO^*$ association complex. It is tempting to simply attribute the higher rate constants measured by us to the higher collision efficiency of Argon compared to Helium. However, based on the following estimates the overall effect is too large. Typically, ratios of 2–3 have been reported for the average energies transferred per collision, $\langle \Delta E \rangle (\text{Ar})/\langle \Delta E \rangle (\text{He})$. To compare the collision efficiencies β_c in the two bath gases, their functional dependence on $\langle \Delta E \rangle$, ⁶⁹

$$\beta_{\rm c}/(1-\beta_{\rm c}^{0.5}) \propto \langle \Delta E \rangle$$
 (15)

as well as the ratio of the Lennard-Jones collision numbers $Z_{\rm LJ}({\rm Ar})/Z_{\rm LJ}({\rm He})$ has to be taken into account. Estimating $\beta_{\rm c}({\rm He}, 298~{\rm K}) \approx 0.25$, a $\langle \Delta E \rangle$ ratio of 2-3 corresponds to $\beta_{\rm c}$ values for Argon that are a factor of 1.5–1.9 higher than the ones for Helium. The effective ratio of the low-pressure limiting rate constants is given by expression (16):

$$\frac{k_0(\mathrm{Ar})}{k_0(\mathrm{He})} = \frac{\beta_{\mathrm{C}}(\mathrm{Ar})Z_{\mathrm{LJ}}(\mathrm{Ar})}{\beta_{\mathrm{C}}(\mathrm{He})Z_{\mathrm{LJ}}(\mathrm{He})} \tag{16}$$

For the Lennard-Jones parameters of allyl peroxy, C_3H_5OO , we assume values of σ = 1.5 Å and ϵ/k_B = 300 K. Consequently, including $Z_{LJ}(Ar)/Z_{LJ}(He) \approx 0.7$ in (16) we expect a ratio in the rate constants of

$$\frac{k_0(Ar)}{k_0(He)} = 1.1 - 1.3$$

hence much lower than the 2–3 ratio in $\langle \Delta E \rangle$. In contrast to this estimate, relying on the high pressure rate constant of Jenkin et al. and adopting the value $F_{\rm c}=0.71$ from Rissanen et al. for the broadening factor F_c, the fall-off fit of our data indicates a four times higher value for the low pressure limiting rate constant $k_0(Ar)$ than that reported for $k_0(He)$ by Rissanen et al.³⁰ The dashed curve in Fig. 8 corresponds to our recommended values k_0 = 2.2 imes 10^{18} cm 6 mol $^{-2}$ s $^{-1}$ and k_∞ = 3.5 imes $10^{11} \text{ cm}^3 \text{ mol}^{-1} \text{ s}^{-1}$ for the pressure dependent room temperature association rate constant of reaction (1) in Argon buffer gas assuming $F_c = 0.71$. Note that in some of the experiments the gas mixtures contained O2 and (COCl)2/propene in the percentage mixing ratio level, which may also have a small effect on the overall pressure dependence. However, O2 collision efficiencies are expected to be similar to those of Ar. Moreover, as the observed rate constants using (COCl)₂/ propene and allyl iodide (the latter at much lower mixing ratio level) are consistent, the presumably higher collision efficiencies of these polyatomic gases were insignificant as well. Along this line of argument, we conclude that the higher rate constants obtained in this work cannot be completely understood by bath gas effects alone but are rather due to unsolved systematic differences in the two experiments. For comparison, in a study of the propyl + O₂ reaction, a similar increase in the rate constant was observed at 4 Torr upon switching from He to N2 for 1-propyl, but no bath gas dependence was found for 2-propyl.⁷³ Unfortunately, due to difficulties to conduct experiments using He as a buffer gas in a cryo-pumped apparatus at a synchrotron radiation beamline, we were not able to perform additional test experiments with He.

Possible sources of error in the experiments are as follows. While the mole fractions of O2 and propene were adjusted by mass flow controllers calibrated for these compounds and are thus accurate to within 1%, the allyl iodide mass flow had to be empirically corrected. In addition, the concentration of the allyl radicals was only determined indirectly based on the determined conversion efficiency of allyl iodide, which was accurate to within 5-10%. However, as oxygen was always used in large excess and as it has been outlined above, inaccuracies in the mole fraction of 2 are expected to play only a minor role. The statistical 2σ standard errors of the fits were in the order of a few percent. Two further sources of error are the pressure in the reactor and the temperature. Readings for p_R are accurate to ± 0.1 mbar or better, *i.e.* from $\pm 19\%$ at 0.8 mbar to $\pm 3\%$ at 3 mbar. A temperature of T = 298 K was assumed for all experiments. However it is possible that the energy deposited by the laser might not be fully equilibrated and the effective gas temperatures can deviate significantly from room temperature. Note that reaction (1) exhibits a negative temperature dependence, hence this effect would cause a negative bias in the rate constants and thus lead to lower values. If the major sources of error are taken into account, the rate constants are estimated to be accurate within $\pm 25\%$.

Conclusions

The allyl + O₂ reaction has been investigated at room temperature and low pressures ranging from 0.8 to 3 mbar. Experiments were conducted in a flow tube reactor coupled to synchrotron radiation to detect reactants and products in a photoelectron/photoion coincidence spectrometer. The reaction was initiated by a Nd:YAG laser that generated allyl from suitable precursors. In all experiments, second-order rate constants k_1 were extracted from kinetic models by taking relevant side reactions into account. At 0.8 mbar $k_1 = 1.40 \times 10^{11} \text{ cm}^3 \text{ s}^{-1} \text{ mol}^{-1}$ was determined using photolysis of allyl iodide at 213 nm to initiate the reaction. Very similar values were obtained at 213 nm and 266 nm photolysis, however the former approach produces radicals more efficiently. Alternatively, we employed the reaction of propene and Cl atoms formed by photolysis of oxalyl chloride to generate allyl. This is a more general approach to produce hydrocarbon radicals, but a large number of secondary reactions have to be considered. Allyl was shown by its mass-selected TPE-spectrum to be the dominant H-atom abstraction product, illustrating the additional information available from PEPICO experiments. When the kinetics is carefully modelled, a rate constant can be obtained that is in good agreement with the one from direct photolysis. The product allyl peroxy was not detected, because it dissociatively photoionises due to its low binding energy in the cation and small Franck-Condon factors close to the ionisation threshold, as indicated by computations. The rate constants determined by us are about a factor of two higher than previously reported values, which can only partly be attributed to the different choice of bath gas (Ar vs. He) and to the neglected side reactions in the work of Rissanen et al. In agreement with their work, the pressure-dependence of the second-order rate constant is consistent with the collisionally stabilised association complex C_2H_5OO being formed as the main reaction product. The fall-off behaviour can be best described by the Troe parameters $k_0=2.2\times10^{18}~\rm cm^6~mol^{-2}~s^{-1},~k_\infty=3.5\times10^{11}~\rm cm^3~mol^{-1}~s^{-1},$ and $F_c=0.71$. When a mixture of propene and oxalyl chloride was used to generate allyl, a second product with an ionisation energy of 8.41 eV is formed, which has been identified in the TPES as 1,3-butadienal. It is most likely formed by the reaction of allyl with the thermally instable, but still abundant OCCl radical.

Conflicts of interest

There are no conflicts to declare.

Acknowledgements

The work was funded by the German Science Foundation DFG through contracts FI575/13-1 and GRK2112. It was also supported by the Swiss Federal Office for Energy (BFE Contract Numbers SI/501269-01). B. Sz. and K. V. gratefully acknowledge funding by the National Science Foundation (CHE-1665464). The authors thank Patrick Ascher for technical support. Experiments were carried out at the VUV beamline of the Swiss Light Source, Paul Scherrer Institute.

Notes and references

- 1 T. W. Schmidt, Int. Rev. Phys. Chem., 2016, 35, 209.
- 2 J. Moses, Icarus, 2000, 143, 244.
- 3 K. Wang, S. M. Villano and A. M. Dean, *Phys. Chem. Chem. Phys.*, 2015, 17, 6255.
- 4 K. Wang, S. M. Villano and A. M. Dean, *Energy Fuels*, 2017, 31, 6515.
- 5 N. Hansen, W. Li, M. E. Law, T. Kasper, P. R. Westmoreland, B. Yang, T. A. Cool and A. Lucassen, *Phys. Chem. Chem. Phys.*, 2010, 12, 12112.
- 6 S. D. Thomas, A. Bhargava, P. R. Westmoreland, R. P. Lindstedt and G. Skevis, *Bull. Soc. Chim. Belg.*, 1996, **105**, 501.
- 7 A. Webster, Mon. Not. R. Astron. Soc., 1993, 265, 421.
- 8 J. Moses, Icarus, 2000, 145, 166.
- 9 V. A. Krasnopolsky, Icarus, 2009, 201, 226.
- 10 L. Vereecken and J. S. Francisco, Chem. Soc. Rev., 2012, 41, 6259.
- 11 A. S. Santiago Olivella, J. Am. Chem. Soc., 2003, 125, 10641.
- 12 D. W. Minsek and P. Chen, J. Phys. Chem., 1993, 97, 13375.
- 13 I. Fischer and P. Chen, J. Phys. Chem. A, 2002, 106, 4291.
- 14 T. Schultz, J. S. Clarke, T. Gilbert, H.-J. Deyerl and I. Fischer, *Faraday Discuss.*, 2000, **115**, 17.
- 15 M. Gasser, A. M. Schulenburg, P. M. Dietiker, A. Bach, F. Merkt and P. Chen, *J. Chem. Phys.*, 2009, **131**, 014304.

- 16 H.-J. Deyerl, T. Gilbert, I. Fischer and P. Chen, J. Chem. Phys., 1997, 107, 3329.
- 17 D. Stranges, M. Stemmler, X. Yang, J. D. Chesko, A. G. Suits and Y. T. Lee, *J. Chem. Phys.*, 1998, **109**, 5372.
- 18 H. E. van den Bergh and A. B. Callear, *Trans. Faraday Soc.*, 1970, **66**, 2681.
- 19 J. M. Tulloch, M. T. Macpherson, C. A. Morgan and M. J. Pilling, *J. Phys. Chem.*, 1982, **86**, 3812.
- 20 A. A. Boyd, B. Noziere and R. Lesclaux, J. Phys. Chem., 1995, 99, 10815.
- 21 L. Seidel, K. Hoyermann, F. Mauß, J. Nothdurft and T. Zeuch, *Molecules*, 2013, **18**, 13608.
- 22 T. M. Selby, G. Meloni, F. Goulay, S. R. Leone, A. Fahr, C. A. Taatjes and D. L. Osborn, *J. Phys. Chem. A*, 2008, 112, 9366.
- 23 J. Lee and J. W. Bozzelli, Proc. Combust. Inst., 2005, 30, 1015.
- 24 C. A. Morgan, M. J. Pilling, J. M. Tulloch, R. P. Ruiz and K. D. Bayes, J. Chem. Soc., Faraday Trans. 2, 1982, 78, 1323.
- 25 R. P. Ruiz, K. D. Bayes, M. T. Macpherson and M. J. Pilling, J. Phys. Chem., 1981, 85, 1622.
- 26 I. R. Slagle, E. Ratajczak, M. C. Heaven, D. Gutman and A. F. Wagner, *J. Am. Chem. Soc.*, 1985, **107**, 1838.
- 27 Z. H. Lodhi and R. W. Walker, J. Chem. Soc., Faraday Trans., 1991, 87, 681.
- 28 N. D. Stothard and R. W. Walker, J. Chem. Soc., Faraday Trans., 1992, 88, 2621.
- 29 M. E. Jenkin, T. P. Murrells, S. J. Shalliker and G. D. Hayman, *J. Chem. Soc., Faraday Trans.*, 1993, **89**, 433.
- 30 M. P. Rissanen, D. Amedro, A. J. Eskola, T. Kurten and R. S. Timonen, *J. Phys. Chem. A*, 2012, **116**, 3969.
- 31 P. Hemberger, M. Lang, B. Noller, I. Fischer, C. Alcaraz, B. K. Cunha de Miranda, G. A. Garcia and H. Soldi-Lose, J. Phys. Chem. A, 2011, 115, 2225.
- 32 P. Hemberger, M. Steinbauer, M. Schneider, I. Fischer, M. Johnson, A. Bodi and T. Gerber, *J. Phys. Chem. A*, 2009, 114, 4698.
- 33 M. Steinbauer, P. Hemberger, I. Fischer and A. Bodi, *Chem-PhysChem*, 2011, 12, 1795.
- 34 E. Reusch, F. Holzmeier, P. Constantinidis, P. Hemberger and I. Fischer, *Angew. Chem., Int. Ed.*, 2017, **56**, 8000.
- 35 C. A. Taatjes, D. L. Osborn, T. A. Cool and K. Nakajima, *Chem. Phys. Lett.*, 2004, **394**, 19.
- 36 C. A. Taatjes, N. Hansen, D. L. Osborn, K. Kohse-Höinghaus, T. A. Cool and P. R. Westmoreland, *Phys. Chem. Chem. Phys.*, 2008, **10**, 20.
- 37 D. L. Osborn, P. Zou, H. Johnsen, C. C. Hayden, C. A. Taatjes, V. D. Knyazev, S. W. North, D. S. Peterka, M. Ahmed and S. R. Leone, *Rev. Sci. Instrum.*, 2008, 79, 104103
- 38 B. Sztáray, K. Voronova, K. G. Torma, K. J. Covert, A. Bodi, P. Hemberger, T. Gerber and D. L. Osborn, *J. Chem. Phys.*, 2017, 147, 013944.
- 39 D. L. Osborn, C. C. Hayden, P. Hemberger, A. Bodi, K. Voronova and B. Sztaray, J. Chem. Phys., 2016, 145, 164202.

- 40 M. Johnson, A. Bodi, L. Schulz and T. Gerber, *Nucl. Instrum. Methods Phys. Res.*, Sect. A, 2009, **610**, 597.
- 41 A. Bodi, P. Hemberger, D. L. Osborn and B. Sztaray, *J. Phys. Chem. Lett.*, 2013, **4**, 2948.
- 42 K. Voronova, K. G. Ervin, K. G. Torma, P. Hemberger, A. Bodi, T. Gerber, D. L. Osborn and B. Sztaray, *J. Phys. Chem. Lett.*, 2018, DOI: 10.1021/acs.jpclett.7b03145.
- 43 W. C. Wiley and I. H. McLaren, *Rev. Sci. Instrum.*, 1955, 26, 1150.
- 44 A. Bodi, B. Sztáray, T. Baer, M. Johnson and T. Gerber, *Rev. Sci. Instrum.*, 2007, **78**, 084102.
- 45 B. Sztáray and T. Baer, Rev. Sci. Instrum., 2003, 74, 3763.
- 46 R. J. Kee, F. M. Rupley and J. A. Miller, *Chemkin-II: A Fortran chemical kinetics package for the analysis of gas-phase chemical kinetics*, Sandia National Laboratories, Livermore, CA, 1989, Report SAND89-8009, 1989.
- 47 A. E. Lutz, R. J. Kee and J. A. Miller, *SENKIN: A Fortran program for predicting homogeneous gas phase chemical kinetics with sensitivity analysis*, Sandia National Laboratories, Livermore, CA, 1990, Report SAND87-8248, 1988.
- 48 R. A. Boschi and D. R. Salahub, Mol. Phys., 1972, 24, 735.
- 49 H. Schmidt and A. Schweig, *Angew. Chem., Int. Ed. Engl.*, 1973, 12, 307.
- 50 J. C. Traeger, Int. J. Mass Spectrom. Ion Processes, 1984, 58, 259.
- 51 T. Schüßler, H.-J. Deyerl, S. Dümmler, I. Fischer, C. Alcaraz and M. Elhanine, *J. Chem. Phys.*, 2003, **118**, 9077.
- 52 G. Meloni, T. M. Selby, F. Goulay, S. R. Leone, D. L. Osborn and C. A. Taatjes, *J. Am. Chem. Soc.*, 2007, **129**, 14019.
- 53 D. L. Baulch, J. Duxbury, S. J. Grant and D. C. Montague, J. Phys. Chem. Ref. Data, 1981, 10, supplement 1.
- 54 O. Welz, M. P. Burke, I. O. Antonov, C. F. Goldsmith, J. D. Savee, D. L. Osborn, C. A. Taatjes, S. J. Klippenstein and L. Sheps, *J. Phys. Chem. A*, 2015, **119**, 7116–7129.
- 55 W. Ludwig, B. Brandt, G. Friedrichs and F. Temps, *J. Phys. Chem. A*, 2006, **110**, 3330.
- 56 M. Ahmed, D. Blunt, D. Chen and A. G. Suits, *J. Chem. Phys.*, 1997, **106**, 7617.
- 57 N. Hemmi and A. G. Suits, *J. Phys. Chem. A*, 1997, **101**, 6633–6637.
- 58 C. Y. Wu, Y. P. Lee and N. S. Wang, *J. Chem. Phys.*, 2004, **120**, 6957.
- 59 C. Y. Wu, Y. P. Lee, J. F. Ogilvie and N. S. Wang, J. Phys. Chem. A, 2003, 107, 2389.
- 60 A. V. Baklanov and L. N. Krasnoperov, J. Phys. Chem. A, 2001, 105, 97.
- 61 B. Gosh, D. K. Papanastasiou and J. B. Burkholder, J. Chem. Phys., 2012, 137, 164315.
- 62 T.-K. Huang, B.-J. Chen, K.-C. Lin, L. Lin, B.-J. Sun and A. H. H. Chang, J. Phys. Chem. A, 2017, 121, 2888.
- 63 D. C. Frost, C. A. McDowell, G. Pouzard and N. P. C. Westwood, J. Electron Spectrosc. Relat. Phenom., 1977, 10, 273.
- 64 P. Masclet, D. Grosjean, G. Mouvier and J. Dubois, *J. Electron Spectrosc. Relat. Phenom.*, 1973, 2, 225.
- 65 S. Mohmand, T. Hirabayashi and H. Bock, *Chem. Ber.*, 1981, **114**, 2609.

- 66 W. Schroeder, M. Monnier, G. Davidovics, A. Allouche, P. Verlaque, J. Pourcin and H. Bodot, *J. Mol. Struct.*, 1989, 197, 227.
- 67 E. W. Kaiser and T. J. Wallington, *J. Phys. Chem.*, 1996, **100**, 9788.
- 68 R. Atkinson, D. L. Baulch, R. A. Cox, J. N. Crowley, R. F. Hampson, R. G. Hynes, M. E. Jenkin, M. J. Rossi and J. Troe, *Atmos. Chem. Phys.*, 2007, 7, 981.
- 69 J. Troe, J. Phys. Chem., 1979, 83, 114.
- 70 T. Lenzer, K. Luther, D. Nilsson and S. Nordholm, *J. Phys. Chem. B*, 2005, **109**, 8325.
- 71 I. Oref and D. C. Tardy, Chem. Rev., 1990, 90, 1407.
- 72 M. Quack and J. Troe, in *Gas Kinetics and Energy Transfer*, ed. P. G. Ashmore and R. J. Donovan, The Chemical Society, 1977, vol. 2.
- 73 R. P. Ruiz and K. D. Bayes, J. Phys. Chem., 1984, 88, 2592.